1678 *Biochemistry* **2010,** *49,* 1678–1688
DOI: 10.1021/bi901693u

BIOCHEMISTRY
including biophysical chemistry & molecular biology
Article

Structure and Ligand Binding Properties of the Epoxidase Component of Styrene Monooxygenase[†,‡]

Uchechi E. Ukaegbu,[§] Auric Kantz,[∥] Michelle Beaton,[∥] George T. Gassner,*[,∥] and Amy C. Rosenzweig*[,§]

[§]*Department of Biochemistry, Molecular Biology, and Cell Biology and Department of Chemistry, Northwestern University, Evanston, Illinois 60208 and* [∥]*Department of Chemistry and Biochemistry, San Francisco State University, San Francisco, California 94132*

Received September 29, 2009; Revised Manuscript Received January 5, 2010

ABSTRACT: Styrene monooxygenase (SMO) is a two-component flavoprotein monooxygenase that transforms styrene to styrene oxide in the first step of the styrene catabolic and detoxification pathway of *Pseudomonas putida* S12. The crystal structure of the N-terminally histidine-tagged epoxidase component of this system, NSMOA, determined to 2.3 Å resolution, indicates the enzyme exists as a homodimer in which each monomer forms two distinct domains. The overall architecture is most similar to that of *p*-hydroxybenzoate hydroxylase (PHBH), although there are some significant differences in secondary structure. Structural comparisons suggest that a large cavity open to the surface forms the FAD binding site. At the base of this pocket is another cavity that likely represents the styrene binding site. Flavin binding and redox equilibria are tightly coupled such that reduced FAD binds apo NSMOA ~8000 times more tightly than the oxidized coenzyme. Equilibrium fluorescence and isothermal titration calorimetry data using benzene as a substrate analogue indicate that the oxidized flavin and substrate analogue binding equilibria of NSMOA are linked such that the binding affinity of each is increased by 60-fold when the enzyme is saturated with the other. A much weaker ~2-fold positive cooperative interaction is observed for the linked binding equilibria of benzene and reduced FAD. The low affinity of the substrate analogue for the reduced FAD complex of NSMOA is consistent with a preferred reaction order in which flavin reduction and reaction with oxygen precede the binding of styrene, identifying the apoenzyme structure as the key catalytic resting state of NSMOA poised to bind reduced FAD and initiate the oxygen reaction.

Flavins are key cofactors in the reductive activation and transfer of oxygen atoms to organic substrates in the biosynthesis of alcohols, aldehydes, and acids (*1*, *2*). Through structural studies, dynamic motions of the flavin isalloxazine ring system have been tracked and linked to discrete catalytic steps associated with substrate binding, oxygenation, and product release (*3*−*8*). Flavin-dependent epoxidations, which are less commonly encountered, have important roles in the biosynthesis of cholesterol and plant pigments and in the styrene catabolic and detoxification pathway of *Pseudomonas* bacteria (*9*−*11*). The soluble flavoenzyme styrene monooxygenase (SMO),[1] which catalyzes the transformation of styrene to *S*-styrene oxide, is readily purified and has proven to be an excellent target for mechanistic studies of flavin-catalyzed epoxidation (*12*−*15*). Studies of SMO have provided some insight into the mechanisms of the functionally related FAD-dependent epoxidases, squalene monooxygenase and zeaxanthin epoxidase, for which practical challenges associated with obtaining reagent quantities of enzyme have limited the extent of previous investigations (*9*, *10*). Structural and mechanistic studies of the enantioselective epoxidation reaction catalyzed by SMO may impact the development of new biological methods for producing chemical building blocks (*16*, *17*) and for removing styrene and styrene oxide from contaminated regions in the environment (*12*).

SMO is composed of two components: a 46 kDa FAD-specific styrene epoxidase (SMOA) and a 20 kDa NADH-specific flavin reductase (SMOB). In catalysis, reduced flavin produced by the reductase must be transferred to the epoxidase active site. The flavin thus takes on roles of substrate and coenzyme in a reaction that is different from that of the single-component flavin monooxygenases such as *p*-hydroxybenzoate hydroxylase (PHBH), in which the flavin reduction and oxygen activation reactions occur within the same polypeptide (*1*, *2*). In the mechanism of SMO, reduced flavin generated by the reductase migrates to the active site of the epoxidase where it is used in the reductive activation of molecular oxygen in the epoxidation reaction (Scheme 1). The efficient transfer of reduced flavin from the reductase to the epoxidase poses a problem since reduced flavin reacts readily with oxidized flavin and molecular oxygen dissolved in solution (*3*).

Various mechanistic strategies for addressing this problem have evolved. Protein−protein interactions between the reductase

[†]This work was supported by National Institutes of Health (NIH) Grants GM070473 (A.C.R.) and GM081140 (G.T.G.). U.E.U. was supported in part by NIH Training Grant GM8061.

[‡]The atomic coordinates (entry 3IHM) have been deposited in the Protein Data Bank.

*To whom correspondence should be addressed. G.T.G.: Department of Chemistry and Biochemistry, San Francisco State University, San Francisco, CA 94132; telephone, (415) 637-1387; fax, (415) 338-2384; e-mail, gassner@sfsu.edu. A.C.R.: Department of Biochemistry, Molecular Biology, and Cell Biology and Department of Chemistry, Northwestern University, Evanston, IL 60208; telephone, (847) 467-5301; fax, (847) 467-6489; e-mail, amyr@northwestern.edu.

[1]Abbreviations: FAD, flavin adenine dinucleotide; ITC, isothermal titration calorimetry; NADPH, nicotinamide adenine dinucleotide phosphate; PHBH, *p*-hydroxybenzoate hydroxylase; rmsd, root-mean-square deviation; SMO, styrene monooxygenase; SMOA, styrene monooxygenase A; SMOB, styrene monooxygenase B; NSMOA, N-terminally histidine-tagged styrene monooxygenase.

 Published on Web 01/07/2010

Scheme 1

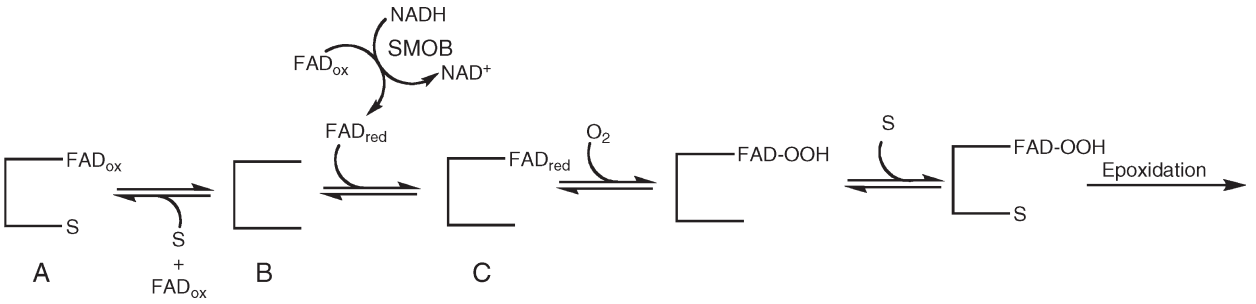

and monooxygenase components of bacterial luciferase and alkane sulfonate monooxygenase are thought to minimize side reactions of freely diffusing flavin with dissolved oxygen and contribute to the efficient transfer of reduced flavin from the reductase to the monooxygenase in catalysis (*18*, *19*), although recent data may not be consistent with a luciferase−oxidoreductase complex (*20*). The reductase of the two-component 4-hydroxyphenylacetate 3-monooxygenase system of *Acinetobacter baumanii* includes an allosteric domain that binds 4-hydroxyphenylacetate and activates the flavin reduction reaction in response to the increasing availability of the hydroxylase substrate. It has been clearly demonstrated that the combination of allosteric regulation with the high affinity of the monooxygenase component for reduced FAD enables the *A. baumanii* system to function efficiently without the need for the formation of a flavin transfer complex in catalysis (*21*).

SMOB is not allosterically regulated in this way, and the reduction and epoxidation reactions of the SMO system are efficiently coupled only when free flavin concentrations are low and the monooxygenase is present in >100-fold molar excess over the reductase (*15*). These features together with sequence homology closely align SMO with 4-hydroxyphenylacetate 3-monooxygenase from *Escherichia coli* W and related proteins (*22*). Numerical simulations modeling steady-state catalysis of SMO suggest a ternary flavin transfer complex may be needed to account for the experimentally observed coupling of the NADH oxidation and styrene epoxidation reactions evaluated over a broad range of FAD concentrations and reductase-to-epoxidase ratios (*15*). However, no direct experimental evidence for protein−protein interactions has been obtained for either styrene monooxygenase or the 4-hydroxyphenylacetate 3-monooxygenase from *E. coli* W (*15*, *23*). A common mechanistic theme for styrene monooxygenase and the 4-hydroxyphenylacetate 3-monooxygenases of *E. coli* W and *A. baumanii* is a thermodynamic linkage of the flavin binding and reduction equilibria that favors the binding of reduced flavin over oxidized flavin with great selectivity (*15*, *21*, *23*). This allows the monooxygenase component of each system to effectively scavenge reduced flavin from solution for use in catalysis.

In this work, we report the crystal structure of the apo form of NSMOA and identify potential substrate and flavin binding pockets. A detailed analysis of the linked redox and ligand binding equilibria presented herein demonstrates a strongly cooperative interaction between substrate analogue (benzene) and oxidized flavin binding equilibria and identifies a significant loss of cooperativity in the reduced FAD complex of NSMOA. The corresponding loss of substrate analogue binding affinity may open the active site to allow oxygen access to react with reduced flavin and supports a preferred reaction order in which the binding and reaction of reduced FAD with oxygen precede the binding of styrene. The equilibrium analysis suggests that in addition to the apo resting state of NSMOA presented here, complexes of apo NSMOA with reduced FAD bound or of NSMOA with oxidized FAD and substrate bound are likely to be the most significant species present in solution prior to reaction of the enzyme with oxygen.

MATERIALS AND METHODS

Protein Purification. N-terminally histidine-tagged styrene monooxygenase (NSMOA) and styrene monooxygenase reductase were purified by Ni affinity chromatography as described previously (*15*). NSMOA was then concentrated to approximately 20 mg/mL by using Centricon-30 ultrafiltration devices (Millipore) and stored in 50% glycerol at −20 °C.

Fluorescence Spectroscopy. Studies were conducted with a Molecular Devices M5 plate reader. N-terminally histidine-tagged SMOA was exchanged into 20 mM MOPSO buffer adjusted to pH 7 by passage through a Biogel P6 desalting column (Bio-Rad). Following buffer exchange, the protein was concentrated by ultrafiltration and combined with buffer containing FAD and/or benzene in a 96-well black-masked Corning-Costar fluorescence microplate. Equilibria were studied by varying the concentration of NSMOA at defined concentrations of FAD and benzene. Samples were excited at 450 nm, and emission was monitored at 520 nm at 25 °C with excitation and emission slit widths of 1 mm.

Oxidation−Reduction Potential Measurements. Equilibrium redox potential measurements were conducted in 20 mM MOPSO (pH 7) over a range of protein concentrations at 25 °C. Spectra of representative redox equilibria of FAD in the presence of NSMOA and reference indicators were recorded with an Ocean Optics USB-2000 spectrophotometer. The solution potential at each point in the titration and the equilibrium midpoint potential of bound FAD in the presence or absence of benzene were computed by using the Nernst equation as described previously (*15*).

Stopped-Flow Fluorescence Spectroscopy. The kinetics of binding of oxidized FAD to NSMOA were measured at 25 °C by using an Applied Photophysics SX17 stopped-flow drive unit fitted with PEEK (polyetheretherketone) valves and tubing. Flavin fluorescence was excited with monochromatic 450 nm light along the 0.1 cm light path of the flow cell. Fluorescence emission was detected along the 1 cm light path of the flow cell with an Edmund Optics VG-6 band-pass filter placed in front of the emission photomultiplier tube. The photomultiplier tube was energized with a Pacific Instruments high-voltage power supply and the signal digitized with a Pico ADC-216 oscilloscope controlled by PicoScope software.

Table 1: Data Collection and Refinement Statistics

	native 1[a]	native 2	Pt1	Pt2	Au
Data Collection					
wavelength (Å)	1.03	0.98	1.05	1.03	1.03
resolution (Å)	50.0 −2.90 (3.00−2.90)	50.0−2.27 (2.31−2.27)	50.0−3.30 (3.42−3.30)	50.0−2.75 (2.80−2.75)	50.0−2.91 (2.96−2.91)
R_{sym}	0.144 (0.405)	0.093 (0.378)	0.107 (0.360)	0.099 (0.386)	0.115 (0.377)
$I/\sigma I$	20 (10.5)	30.9 (6.5)	23.4 (9.4)	19.0 (5.8)	28 (7.9)
completeness (%)	100 (100)	100 (100)	99.7 (99.4)	98.9 (100)	100 (100)
redundancy	11.4 (11.5)	11.6 (11.6)	10.0 (9.6)	5.7 (5.8)	11.5 (11.6)
Refinement					
resolution	42.4−2.30				
no. of reflections	43907				
R_{work}/R_{free}	0.21/0.24				
no. of atoms					
protein	6429				
water	578				
average B factor (Å^2)	18.9				
root-mean-square deviation					
bond lengths (Å)	0.006				
bond angles (deg)	0.891				

[a]The native 1 data set was collected at the GM/CA-CAT beamline; all others were collected at LS-CAT beamlines.

Isothermal Titration Calorimetry (*ITC*). ITC measurements were conducted at 25 °C in 20 mM MOPSO buffer (pH 7) using a MicroCal VP-ITC instrument. In these studies, apo NSMOA was placed in the sample cell of the calorimeter and titrated with benzene dispensed from the autotitrator syringe set to stir at 307 rpm. To establish the heat of dilution of benzene, a series of injections of benzene were made under identical conditions into MOPSO buffer that contained no enzyme. Enthalpy changes corresponding to the NSMOA−benzene association equilibrium were then computed by numerical integration of the raw ITC data and fit with a single-site model using Origin version 7.

Crystallization. NSMOA samples were dialyzed overnight into 20 mM MOPS (pH 7.0) and 5% glycerol prior to crystallization. Samples were pooled and concentrated using an Amicon 10 kDa centrifugal device (Millipore) to concentrations as high as 80 mg/mL. The histidine tag was not removed. Ligand-free crystals of NSMOA appeared within 2 days by mixing equal volumes of protein at a concentration of 22.9 mg/mL and a reservoir solution consisting of 0.2 M $MgCl_2$, 0.1 M Tris-HCl (pH 8.5), and 30% (w/v) PEG 4000. All NSMOA crystals were transferred to 10 μL drops that included the precipitant and 15% (v/v) PEG 400 as a cryoprotectant and immediately flash-cooled in liquid nitrogen.

Substrate Analogue Soaks and Cocrystallization. Several soaking and cocrystallization protocols were developed in an attempt to obtain structures of the flavin- and substrate analogue-bound forms of NSMOA. Efforts to obtain a reduced $FADH_2$-bound structure included soaking crystals for 5−25 min in solutions containing 0.1−1.0 μM SMOB in the presence of 0.5−50 mM FAD and 2−100 mM NADH. In addition, crystals were soaked in solutions containing 10−50 mM FAD and 10 mM sodium dithionite. Crystallization of NSMOA in the presence of varying concentrations of SMOB, FAD, NADH, and dithionite was attempted both aerobically and in a Coy anaerobic chamber. Finally, solutions (1 μL) containing 10 mM FAD and 100 μM to 10 mM benzene were added to the crystallization drops for 15 min to 24 h in an effort to obtain crystals of oxidized, substrate analogue-bound NSMOA.

Data Collection. Diffraction data were collected at 100 K using Mar225 and Mar300 CCD detectors at LS-CAT (sector 21) beamlines ID-D and ID-F and at GM/CA-CAT (sector 23) beamline ID-D at the Advanced Photon Source (APS, Argonne National Laboratory, Argonne, IL). The data sets were indexed, integrated, and scaled with HKL2000 (*24*). There are two molecules in the asymmetric unit, and the crystals belong to space group $P6_3$ with the following unit cell dimensions: $a = b =$ 114.302 Å, and $c =$ 140.803 Å. Diffraction data statistics are listed in Table 1.

Structure Determination. The structure was determined by multiple isomorphous replacement with anomalous scattering (MIRAS) phasing with autoSHARP (*25*). We obtained three heavy atom derivatives by soaking crystals in 10 and 28.9 mM K_2PtCl_4 (Pt1 and Pt2, respectively, in Table 1) and 1 mM $KAu(CN)_2$ (Au in Table 1) for 24 h. The heavy atom solutions (1 μL) were added directly to each drop. SHELXD in autoSHARP located 20 Pt and 10 Au sites, and an initial experimental map was calculated to 2.75 Å resolution using the data obtained for the 28.9 mM K_2PtCl_4 soak as the native data set (Pt2 in Table 1) (*25*−*27*). The phasing powers for the derivatives were 1.124 for Pt1, 1.246 for Pt2, and 0.87 for Au. The map was improved by solvent flattening using SOLOMON in autoSHARP with an estimated solvent content of 49.1% (*28*). The initial figure of merit was 0.50, and the figure of merit after solvent flattening was 0.90.

Model Building and Refinement. An initial model was generated using Buccaneer (*29*) and was further adjusted manually in Coot (*30*). This model was subjected to iterative rounds of refinement and rebuilding in Refmac5 (*31*) and Coot, respectively, using data set Pt2. A higher-resolution native data set was then obtained using a crystal that had been soaked in a solution containing 10 mM FAD and 100 μM benzene for 24 h (native 2 in Table 1). The 2.75 Å resolution model ($R_{work} = 0.21$, and $R_{free} =$ 0.26) was used as a molecular replacement model in PHASER (*32*), and further refinement to 2.3 Å resolution was

conducted with Refmac5 (Table 1). The final model consists of residues 3−410 in chain A, residues 4−410 in chain B, and 578 water molecules. A Ramachandran plot calculated with PROCHECK (*33*) shows that 96.3% of the residues have the most favorable geometry with the rest in additionally allowed regions. Figures were generated with PyMOL (*34*). Coordinate superpositions were performed using LSQKAB (*35*) or the SSM server (http://www.ebi.ac.uk/msd-srv/ssm) (*36*). Protein−protein interfaces were analyzed with PROTORP (http://www.bioinformatics.sussex.ac.uk/protorp). Cavity calculations were performed with CASTp (*37*), and sequence alignments were prepared with ALINE (*38*).

RESULTS

Estimation of Benzene Binding Affinity by Isothermal Titration Calorimetry. It was previously demonstrated that benzene binds to SMOA during catalytic turnover as a competitive inhibitor (*15*), and in this work, we use benzene as a nonreactive substrate analogue of styrene in the evaluation of the ligand binding and redox equilibria of NSMOA under aerobic and anaerobic conditions. Substitution of benzene for styrene in these studies prevented problems associated with the oxidation and polymerization of styrene, and protein modification through alkylation. These effects are amplified in equilibrium studies that require long-term exposure of NSMOA to high concentrations of styrene. In addition to providing new insight into the role of ligand binding in the reaction mechanism of NSMOA, the equilibrium dissociation constants of benzene and oxidized and reduced forms of FAD helped us establish the concentration ranges to explore in crystallographic studies.

The affinity of binding of benzene to the apoenzyme was measured by ITC by titration of apo NSMOA with a concentrated stock solution of benzene. After correction for the heat of dilution, data were fit according to a noninteracting site equilibrium model, which assumes one benzene-binding site per NSMOA monomer (Figure 1). The best fit through these data indicates that the equilibrium dissociation constant of apo NSMOA for benzene is quite weak (K_{d1} = 4.20 ± 0.37 mM).

Measurement of Linked Benzene and FAD Binding Equilibria by Fluorescence Titration. The interaction of oxidized FAD and NSMOA was investigated at equilibrium by monitoring the increase in steady-state fluorescence associated with the binding of the flavin. Since oxidized FAD binds weakly to NSMOA, it was necessary to include relatively high concentrations of FAD and NSMOA in the titration. The Molecular Devices M5 fluorimeter was found to have a linear fluorescence response up a concentration of 50 μM FAD. Above this concentration, the signal became complicated by the inner filter effect, so the FAD concentration was not further increased. Benzene was used in these studies in place of styrene because of the favorable stability and solubility characteristics of this substrate analogue.

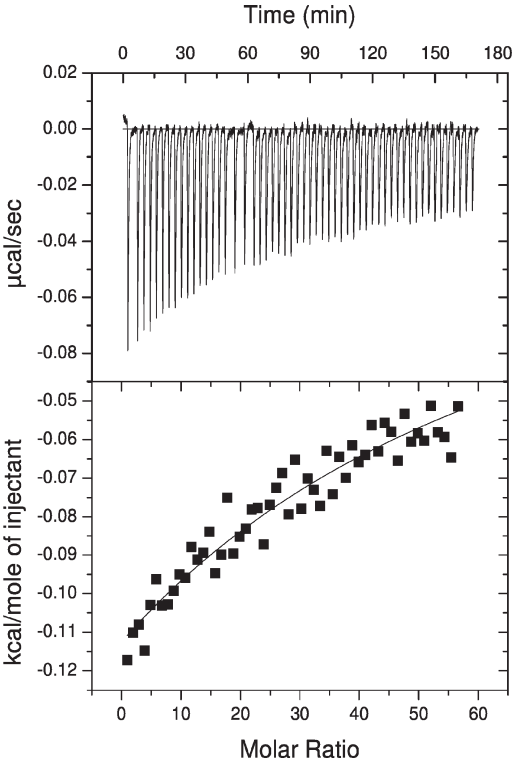

FIGURE 1: Calorimetric titration of apo NSMOA with benzene. The top panel shows raw data corresponding to 54 5 μL injections of 5 mM benzene into 18 μM NSMOA monomer in 20 mM MOPSO buffer (pH 7) at 25 °C. The bottom panel shows a least-squares fit with a single, noninteracting site model. Parameters from this fit are as follows: $\Delta G = -3.24 \pm 1.7$ kcal/mol, $\Delta H = -26.17 \pm 1.9$ kcal/mol, and $\Delta S = -77 \pm 40$ cal/mol·K.

When it binds NSMOA, the fluorescence of FAD increases, and eq 1 was derived and used to compute the apparent binding constant of FAD in the presence of various benzene concentrations, where ε_1 and ε_2 are the molar extinction coefficients for the fluorescence of free and bound forms of FAD, respectively. Fits passing through the titration data are shown in the inset of Figure 2. Use of higher concentrations of NSMOA proved to be experimentally problematic, and for this reason, it was not possible to record data further into the saturation region of the binding isotherm. This limitation prevented calculation of the end point of the titration in the equilibrium reaction of apo NSMOA with FAD. However, the linkage of the benzene and FAD binding equilibria causes the apparent K_d of FAD to decrease hyperbolically such that data from titrations that included benzene could be fit to yield good estimates of ε_2 and the apparent K_d. The data plotted in Figure 2 were fit with eq 2, which describes the dependence of the apparent K_d of oxidized FAD on the benzene concentration and the equilibrium dissociation constants of apo NSMOA interacting with benzene (K_{d1}) and FAD (K_{d3}) and the oxidized FAD−NSMOA complex interacting with benzene (K_{d4}).

$$F = \varepsilon_1[\mathrm{FAD}]_{\mathrm{total}} + \left[\frac{K_d^{\mathrm{app}} + [\mathrm{FAD}]_{\mathrm{total}} + [\mathrm{SMOA}]_{\mathrm{total}} - \sqrt{(K_d^{\mathrm{app}} + [\mathrm{FAD}]_{\mathrm{total}} + [\mathrm{SMOA}]_{\mathrm{total}})^2 - 4[\mathrm{FAD}]_{\mathrm{total}}[\mathrm{SMOA}]_{\mathrm{total}}}}{2}\right](\varepsilon_2 - \varepsilon_1) \quad (1)$$

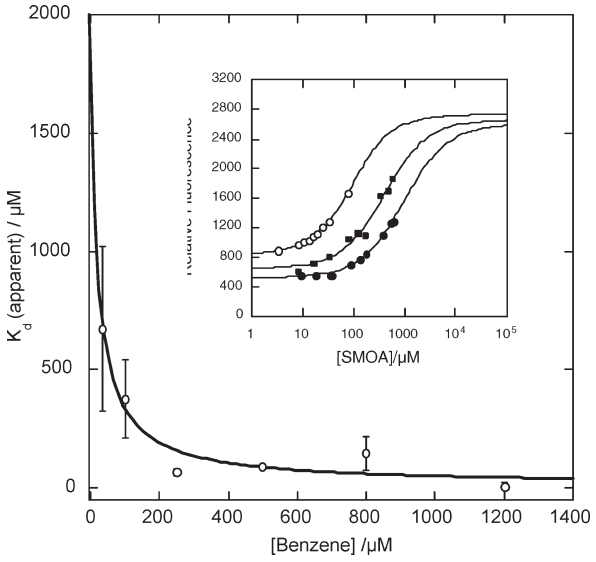

FIGURE 2: Estimate of K_d for oxidized FAD binding to NSMOA in the presence of a saturating level of benzene. Solutions containing 50 μM oxidized FAD and 0−1.2 mM benzene were titrated with NSMOA. The inset shows raw data from titrations at 35 (●), 100 (■), and 250 (○) μM benzene fit with the quadratic equation described in the text to yield apparent K_d values. Apparent K_d values plotted as a function of benzene concentration were then fit to find the best estimates of the K_d value of oxidized FAD for NSMOA in the presence and absence of a saturating level of benzene.

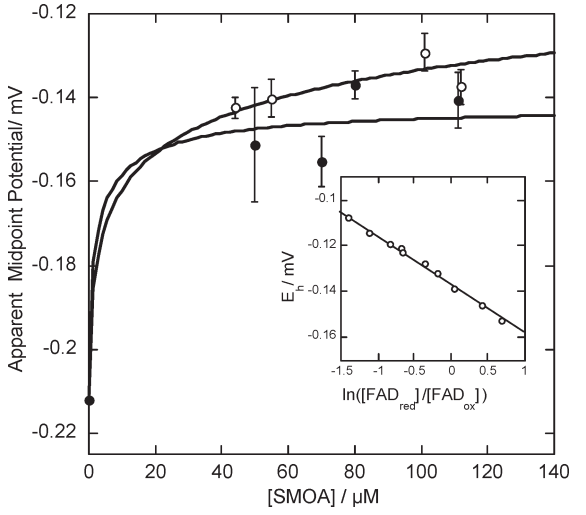

FIGURE 3: Estimates of NSMOA-bound FAD equilibrium redox potential in the presence (●) and absence (○) of 1.2 mM benzene. Apparent FAD midpoint potentials are plotted as a function of the NSMOA concentration at which they were determined. The inset shows an example of the solution potential data used to compute the apparent midpoint potential at 80 μM NSMOA.

$$K_d^{app} = \frac{K_{d3}\left(1+\frac{[B]}{K_{d1}}\right)}{1+\frac{[B]}{K_{d4}}} \quad (2)$$

The best hyperbolic fit through these data imposing the value of K_{d1} determined in the ITC experiment gives limiting values of 1.57 ± 0.79 mM for K_{d3} and 26 ± 20 μM for K_{d4}.

Redox Measurements. Apparent equilibrium midpoint potentials were computed after spectral deconvolution by using

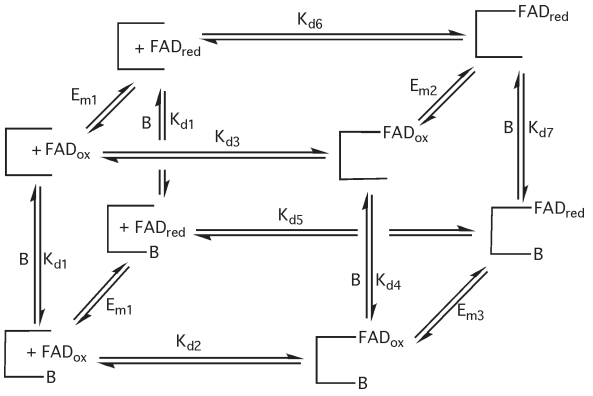

FIGURE 4: Ligand binding and redox equilibria of NSMOA. Equilibrium dissociation constants are as follows: K_{d1} = 4.20 ± 0.37 mM for the interaction of benzene with apo NSMOA measured by ITC; K_{d2} = 26 ± 20 μM and K_{d3} = 1.57 ± 0.79 mM for the binding of oxidized FAD to the benzene-bound and apo forms of NSMOA, respectively, as determined by fluorescence titration; K_{d5} = 112 ± 30 nM and K_{d6} = 206 ± 27 nM for the binding of reduced FAD to the benzene-bound and apo forms of NSMOA, respectively, as determined by electrochemical titration; K_{d4} = 69.6 ± 64 μM and K_{d7} = 2.3 ± 1.9 mM for the binding of benzene to the reduced and oxidized FAD complexes of NSMOA, respectively, computed from linkage relationships ($K_{d4} = K_{d1}K_{d2}/K_{d3}$, and $K_{d7} = K_{d1}K_{d5}/K_{d6}$). The solution potential of free FAD (E_{m1}) equals −212 mV (*15*). The equilibrium midpoint potentials of FAD bound to the benzene-free and bound forms of NSMOA calculated from the linkage relationships $E_{m2} = E_{m1} - RT/nF \times \ln(K_{d2}/K_{d5})$ and $E_{m3} = E_{m1} - RT/nF \times \ln(K_{d3}/K_{d6})$ are −97 and −142 mV, respectively.

the Nernst equation as described previously (*15*). Since FAD binds reversibly to NSMOA, both FAD-bound and FAD-free populations were considered in the analysis of redox equilibria. This was accomplished by conducting redox titrations over a range of NSMOA concentrations. These studies were completed in the presence or absence of benzene to further establish the linkage of the flavin reduction and benzene binding equilibria. The apparent midpoint potentials plotted in Figure 3 were fit with eqs 3 and 4, which give the dependence of the apparent midpoint potential on the concentration of NSMOA for titrations, which excluded and included benzene, respectively.

$$E_m^{app} = E_m^{freeFAD} + \frac{RT}{nF}\ln\left(\frac{1+\frac{[NSMOA]}{K_{d6}}}{1+\frac{[NSMOA]}{K_{d3}}}\right) \quad (3)$$

$$E_m^{app} = E_m^{freeFAD} + \frac{RT}{nF}\ln\left(\frac{1+\frac{[NSMOA]}{K_{d5}}}{1+\frac{[NSMOA]}{K_{d2}}}\right) \quad (4)$$

Known values for the solution potential of free FAD ($E_m^{free\ FAD}$) and the equilibrium dissociation constants for oxidized FAD binding to the benzene-bound (K_{d2}) and apo (K_{d3}) forms of NSMOA, which were determined by fluorescence titration (Figure 2), were included as fitting constants. In this way, it was possible to compute estimates for the remaining dissociation constants (K_{d5} = 112 ± 30 nM, and K_{d6} = 206 ± 27 nM) describing the binding equilibria of reduced FAD interacting with the benzene-free and benzene-bound forms of NSMOA, respectively. The linkages of the redox and ligand

binding equilibria of NSMOA are summarized in Figure 4 together with numerical estimates of the corresponding equilibrium midpoint potentials and ligand dissociation constants.

Flavin Binding Kinetics. The binding of oxidized FAD to NSMOA monitored by stopped-flow fluorescence spectroscopy is shown in Figure 5. The binding reaction studied under pseudo-first-order reaction conditions results in three kinetic phases characterized by two initial rapid increases followed by a slow decrease in fluorescence emission intensity. Data shown in the plot were subjected to a logarithmic time averaging scheme to improve the signal-to-noise ratio and to optimize the data spacing for exponential fitting.

Crystal Structure. The structure of NSMOA was refined to 2.3 Å resolution (Table 1). An N-terminal histidine tag was not visible in the electron density map. Many of the side chains were visible in the MIRAS experimental map, and most had well-defined electron density in the final $2F_o - F_c$ map. The NSMOA monomer comprises two globular domains spanned by a long α-helix (Figure 6A). Domain A consists of a four-stranded parallel β-sheet (β1, β2, β5, and β6) flanked by helices α1, α5, and α6 as well as two 3_{10}-helices, α2 and α7. A β-hairpin formed by β12 and β13, helix α12, and the N-terminal part of helix α13 can also be considered part of this domain. Domain B includes a seven-stranded mixed β-sheet (β3, β4, and β7−β11) flanked by helices α8−α11 on one side and the C-terminus of α13 and helices α14−α17 on the other. The two NSMOA molecules in the asymmetric unit form a homodimer (Figure 6B), consistent with gel filtration analysis (*14*). The two monomers are very similar and superpose with a rmsd of 0.31 Å for 407 Cα coordinates. The interface region, which buries 1034 Å^2 per monomer, consists primarily of loop regions along with 3_{10}-helices α2 and α9 and helix α6. Despite extensive soaking and cocrystallization experiments involving FAD, $FADH_2$, and benzene at concentrations demonstrated to bind to NSMOA in the solution studies, no electron density attributable to benzene or FAD was detected in $F_o - F_c$ maps.

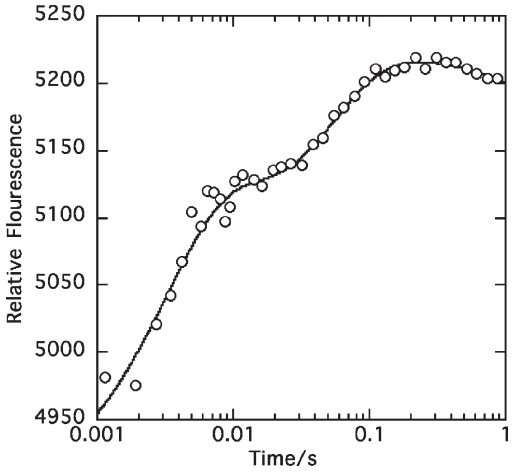

FIGURE 5: Kinetics of oxidized FAD binding to NSMOA monitored by stopped-flow fluorescence spectroscopy. A solution of 280 μM NSMOA was rapidly mixed with 50 μM FAD in the stopped-flow cell. A four-exponential fit through the data yields the following estimated rate constants: $k_1 = 265\ s^{-1}$, $k_2 = 120\ s^{-1}$, $k_3 = 21\ s^{-1}$, and $k_4 = 0.34\ s^{-1}$.

DISCUSSION

Structural Comparisons. Searches with the DALI server (*39*) indicate that NSMOA is most similar to PHBH from *Pseudomonas fluorescens*. Although structures of the hydroxylase components from two two-component systems have been determined recently (*40*, *41*), the single-component PHBH is a better structural match. Superposition with the PHBH Phe161Ala variant structure (Protein Data Bank entry 1CC4, top hit in a DALI search) (*42*) yields an rmsd of 2.47 Å for 309 Cα coordinates. This mutant and the related Arg166Ser variant were prepared to probe the roles of these residues in NADPH binding by PHBH. NSMOA also closely resembles PHBH from *Pseudomonas aeruginosa* (*4*). Superposition of NSMOA and PHBH shows that the cores of both domains are similar, with some significant differences on the periphery of the molecule and

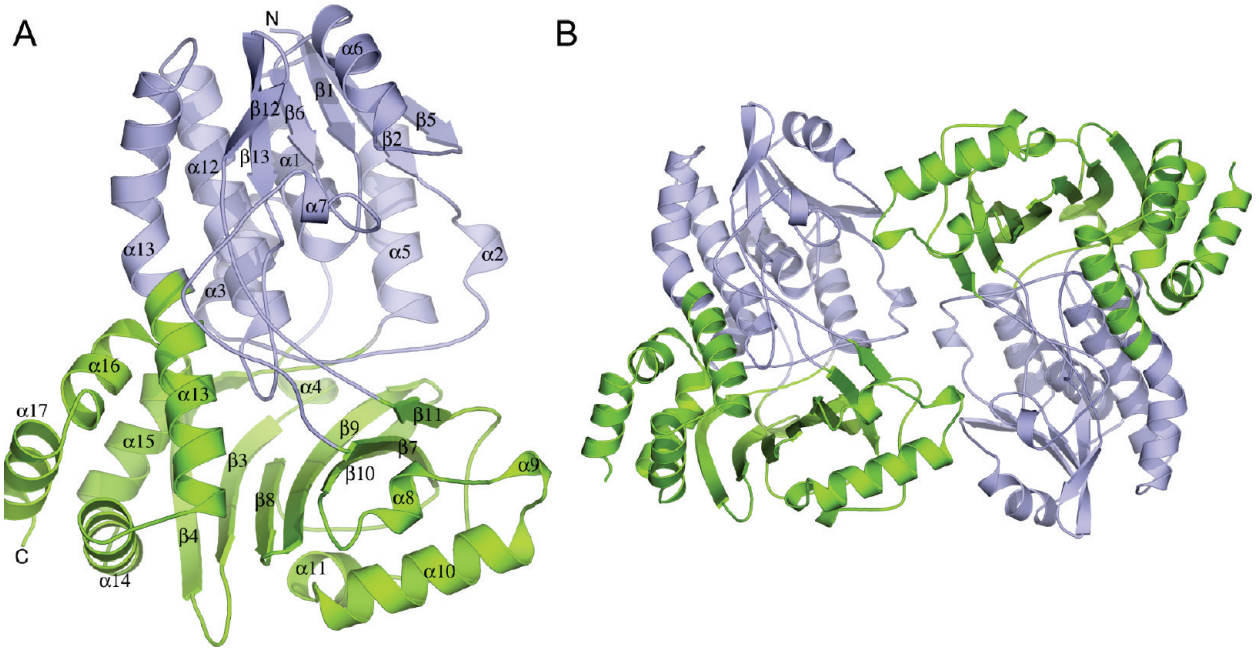

FIGURE 6: Overall structure of NSMOA. (A) NSMOA monomer. Domain A is colored blue and domain B green. Secondary structure elements are labeled. (B) NSMOA dimer colored as in panel A.

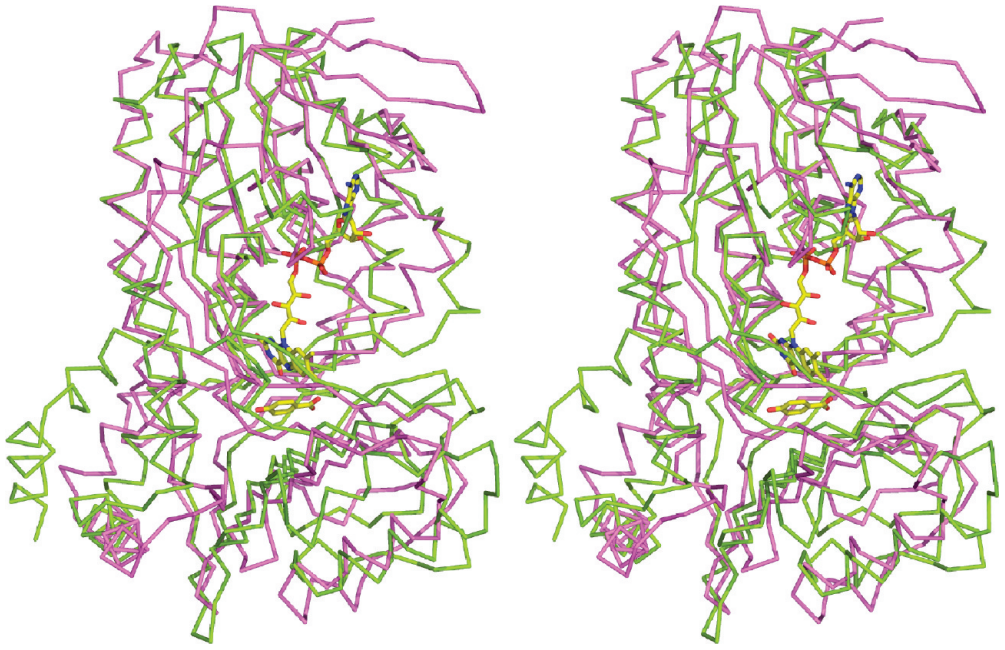

FIGURE 7: Stereosuperposition of NSMOA (green) and PHBH (magenta, Protein Data Bank entry 1CC4). The FAD and *p*-hydroxybenzoate bound to PHBH are shown as sticks.

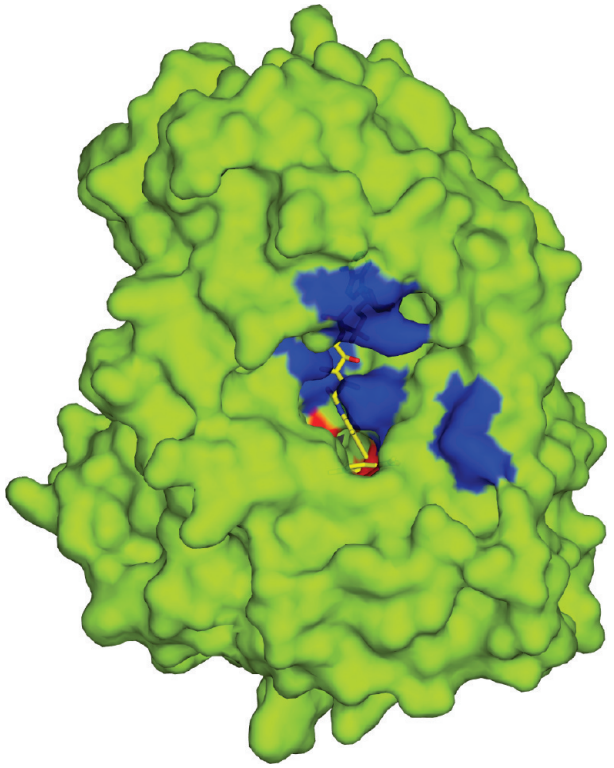

FIGURE 8: Surface representation of NSMOA with FAD and *p*-hydroxybenzoate from the PHBH structure superposed. Positions of residues predicted to interact with FAD are colored blue, and positions of residues in the predicted substrate-binding pocket are colored red. The FAD and substrate binding pockets are surface accessible.

in loop regions (Figure 7). For example, there is an insertion in PHBH domain A that forms a β-hairpin near helix α6 in NSMOA. This β-hairpin is also present in other homologues, including the flavin hydroxylase RebC (*43*). In addition, the C-terminus of NSMOA is more extended and includes additional helices not present in PHBH. The regions connecting domains A and B also differ somewhat, with residues 152−166 in NSMOA forming a loop, whereas the corresponding region in PHBH is an extended β-strand. Although PHBH is also dimeric in solution, it crystallizes with one monomer in the asymmetric unit. Two interfaces between symmetry-related molecules are observed in its structure (*44*), of which neither resembles the NSMOA dimer interface.

Flavin Binding Site. Despite extensive efforts, a structure in the presence of $FADH_2$ or FAD and benzene was not obtained. The FAD binding cavity can be identified by comparison to the PHBH structure, however (Figures 7 and 8). In the location of the FAD in PHBH (*45*), NSMOA has a large cavity that could accommodate FAD and is open to the surface (Figure 8), which would allow transfer of reduced $FADH_2$ from SMOB. Similar to PHBH, the isoalloxazine ring is predicted to reside at the interface between the two domains with the ribityl group and adenosine ring extending into domain A. The cavity is occupied by a number of water molecules in the current structure. In PHBH, the flavin ring interacts with residues Gly 46, Val 47, Gly 298, Leu 299, and Asn 300. Residues Val 48, Ala 49, Gly 307, Ala 308, and Asn 309 occupy these positions in NSMOA (Figure 9). The carbonyl oxygen of Ala 308 is oriented nearly identically to that of Leu 299 in PHBH, suggesting it may interact with both ribose position O3′ and the flavin carbonyl O2 atom. Residue Asn 309 in NSMOA may also be involved in hydrogen bonding with the flavin carbonyl O2 atom. Residue Asp 295 in NSMOA occupies a position similar to that of PHBH Asp 286, which interacts with the ribityl chain.

There are also a number of differences between NSMOA and PHBH in this putative FAD binding site. The NSMOA main chain adopts a different conformation from PHBH spanning residues 32−46. As a result, Arg 43 and Asn 46, which are equivalent to Arg 42 and Arg 44 of PHBH, respectively, of which both are involved in FAD binding, are not properly positioned to interact with FAD. Additionally, differences in secondary structure cause NSMOA residues Lys 145 and Tyr 146 to extend into the pocket where they would interfere with binding of

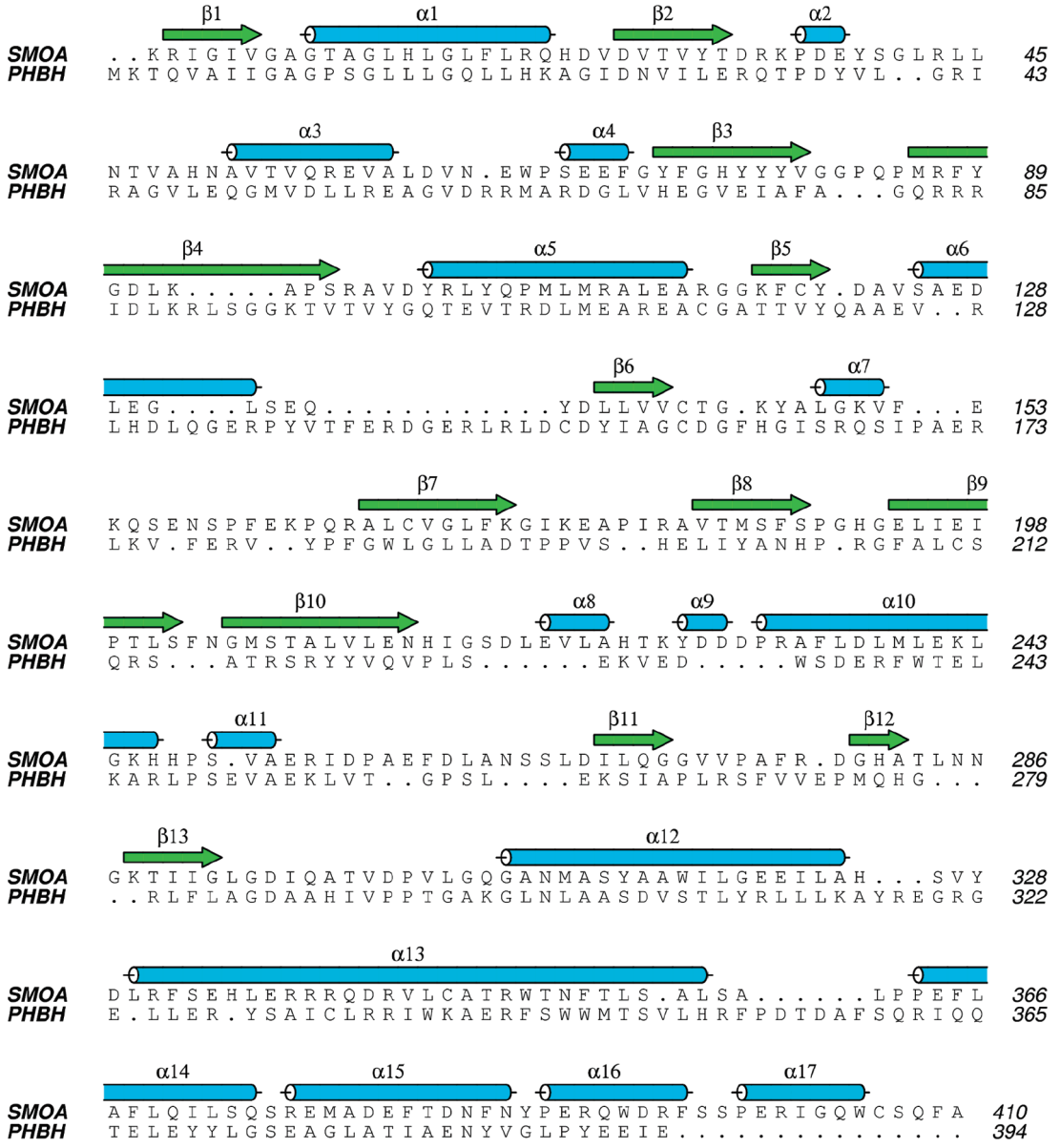

FIGURE 9: Structure-based sequence alignment of SMOA and PHBH. The secondary structure elements for SMOA are indicated.

the adenosine ring. However, the orientation of the adenosine ring observed in the structure of *Comamonas testosteroni* 3-hydroxybenzoate hydroxylase (*46*) can be accommodated by the NSMOA structure. Finally, Ser 13 within the first helix of PHBH, which interacts with the pyrophosphate group, is replaced with alanine in NSMOA. Several residues adjacent to the flavin binding site in PHBH, including Phe 161, His 162, Arg 166, and Arg 269, are important for NADPH binding (*8*, *42*). These residues are not conserved in NSMOA, and the corresponding regions adopt completely different conformations, consistent with NSMOA not interacting directly with pyridine nucleotides.

Substrate Binding Site. At the bottom of the FAD binding site, a likely substrate binding cavity is present (Figure 8). This cavity is located in a position analogous to that of the *p*-hydroxybenzoate site in PHBH (*42*) and is large enough to accommodate styrene. The pocket is adjacent to the position where the FAD isoalloxazine ring is predicted to sit and abuts the surface of the seven-stranded β-sheet in domain B. The putative substrate binding site is completely buried within the protein core, with the only access via the FAD binding site. A number of hydrophobic residues, including Val 184, Met 186, Ile 196, Ile 198, Val 211, Gly 305, Phe 382, and Phe 386, line the cavity (Figure 10). Also surrounding the pocket are His 76, Tyr 78, Gln 306, and Asn 309. Previous predictions of the styrene binding site based on computational modeling identified residues Phe 235, Val 303, Leu 220, Ile 198, and Val 222 as surrounding the styrene (*47*). Of these residues, only Ile 198 is present in the cavity in our structure. Val 303 is nearby; however, its side chain points away from the pocket, and the remaining residues are quite distant. In PHBH, residue Pro 293 interacts with the 3-OH group of the product and is thought to stabilize the transition state (*48*). The analogous residue in NSMOA, Pro 302, occupies the same position but cannot engage in the same way with the styrene ring in the substrate epoxidation reaction. Other residues involved in binding *p*-hydroxybenzoate include Arg 214, Arg 220, and Tyr 201 which are replaced with Thr 200, Ala 209, and Met 186 in NSMOA, respectively. This increase in hydrophobicity is consistent with binding styrene. The active site residue His 72, which is thought to function in a proton relay from solvent to the aromatic ring hydroxyl of *p*-hydroxybenzoate (*49*), corresponds

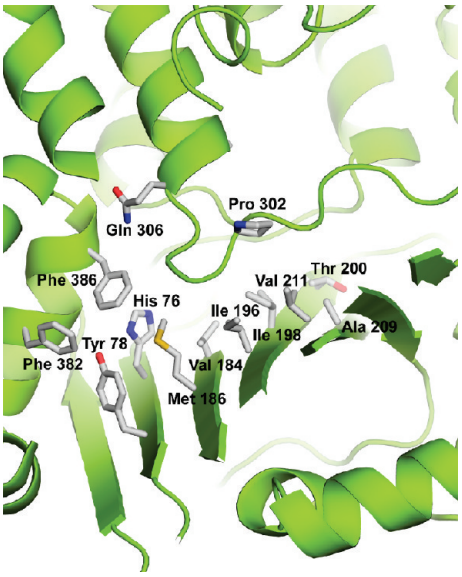

FIGURE 10: Residues lining the proposed styrene binding pocket in NSMOA.

to Tyr 73 and Phe 74 in NSMOA. Other differences along the proton relay path identified in the PHBH structure include the substitution of Phe 386 for Tyr 385 of PHBH and Val 210 for Tyr 222 of PHBH. The presence of non-hydrogen bonding side chains in these positions suggests that NSMOA does not employ the same type of proton shuttle system that has been invoked in the PHBH mechanism.

Crystallographic and kinetic data have resolved three conformations of PHBH, which are thought to be relevant to catalysis (*1*, *48*). Two of these arrangements, designated "in" (Protein Data Bank entry 1PBE) (*45*) and "out" (Protein Data Bank entry 1DOD) (*4*), differ primarily in the position of the isoalloxazine ring, which has moved to more sequestered and solvent-exposed locations, respectively. In addition, *p*-hydroxybenzoate is bound in the flavin in structure, whereas the flavin out structure contains the reaction product, 3,4-dihydroxybenzoate. In a third structure, termed "open" (Protein Data Bank entry 1K0I) (*8*), a more substantial movement of protein allows substrate and product access to the active site. Given substantial differences in regions bordering the binding sites (e.g., NSMOA residues 123−126, 143−146, and 268−275) (Figure 7), it is difficult to compare NSMOA to these subtle variants. However, it is clear that the FAD is exposed to solvent and that the predicted substrate binding cavity is not. Therefore, the current structure may be comparable to the flavin out conformation.

Catalytic Significance of the Apoenzyme and Complexes with Substrate and FAD. The intracellular concentration of oxidized FAD is estimated to be less than 100 μM (*23*), and the growth of *Pseudomonas putida* S12 is inhibited at styrene concentrations greater than 300 μM (*50*), indicating that intracellular oxidized flavin and styrene concentrations are likely to be low relative to the millimolar equilibrium constants determined in this study for interaction with apo NSMOA. This suggests that the apoenzyme structure reported here represents a significant fraction of SMOA present in solution under typical cellular conditions.

Oxidized FAD and benzene binding equilibria of NSMOA are strongly linked, such that the binding of each increases the affinity of NSMOA for the other by ~60-fold on the basis of the K_{d1}/K_{d4} or K_{d3}/K_{d2} ratios (Figure 4); therefore, if both substrate and oxidized FAD are present in solution, they will cooperatively bind the enzyme with a much higher affinity. Thus, in addition to the apoenzyme, NSMOA with both oxidized FAD and styrene bound is expected to be present in the cell. Complexes of NSMOA with only FAD or styrene bound are expected to represent a much smaller fraction of the total enzyme.

Flavin reduction is linked to an ~8000-fold increase in the flavin binding affinity of the apoenzyme (K_{d3}/K_{d6}), but there is an only ~200-fold increase in flavin binding affinity for the NSMOA−benzene complex (K_{d2}/K_{d5}). In either case, we can conclude that reduced FAD not only binds tightly to NSMOA but also competitively displaces oxidized FAD from the enzyme regardless of whether the substrate analogue is bound.

The substrate analogue binds the reduced FAD complex of NSMOA with an affinity that is only ~2 times greater than its affinity for the oxidized FAD complex (K_{d1}/K_{d7}). This 30-fold decrease in the cooperativity of substrate analogue and reduced FAD binding equilibria translates into a substrate analogue binding affinity for the reduced FAD complex of NSMOA that is only ~2 times greater than that observed for the oxidized FAD complex ($K_{d7} \sim 2.3$ mM vs $K_{d7} \sim 4.2$ mM). This interaction is too weak to account for the catalytic activity of NSMOA, which has an apparent K_m of 5 μM for styrene and a K_i for benzene of 170 μM (*15*). For this reason, the complex of NSMOA with reduced FAD and styrene bound is expected to represent a relatively small fraction of the total forms of enzyme present during catalysis.

Functional Implications. Giving consideration to both the physiologically relevant concentration ranges of substrate and FAD and the observed linkage of ligand binding and redox equilibria in this system, we can conclude that the four most catalytically relevant states of the enzyme prior to its reaction with molecular oxygen are those shown in Scheme 1. The complex with substrate and oxidized FAD (A) forms in a strongly cooperative fashion and may represent a means of buffering the intracellular oxidized FAD concentration and maintaining styrene in the vicinity of the active site while NSMOA is awaiting the arrival of reduced FAD. The cooperative linkage of oxidized FAD and substrate analogue NSMOA binding equilibria indicates the apoenzyme structure (B) will be a predominant form of the enzyme under conditions when reduced FAD is absent. The fraction of the enzyme having only substrate or oxidized FAD bound will be less significant under these conditions. Reduced FAD binds with very high affinity to apo NSMOA and will also easily competitively displace oxidized FAD from the complex of enzyme with substrate and oxidized FAD. The reduced FAD enzyme complex (C) has a very low affinity for substrate, such that in the presence of reduced FAD, only a small fraction of the enzyme will be present as a reduced FAD and substrate-bound complex. Clearance of substrate from the active site may be necessary to allow oxygen access to react with the reduced FAD in the catalytic mechanism. We can conclude that the crystal structure presented here represents one of the three most catalytically relevant states of the enzyme prior to its reaction with molecular oxygen.

The kinetics of tracking the binding of oxidized FAD to NSMOA by stopped-flow fluorescence spectroscopy strongly support the idea that binding of oxidized flavin to NSMOA involves at least three steps corresponding to changes in the flavin electronic environment. Part of the investment in binding energy associated with the formation of the low-affinity oxidized FAD−NSMOA complex may be in the conformational reorganization of the FAD

binding pocket of apo NSMOA into a configuration that accommodates the binding of FAD. The details of these interactions will have to await the outcome of future structural studies.

ACKNOWLEDGMENT

Northwestern University is a member institution of the Life Sciences Collaborative Access Team (LS-CAT) at sector 21 of the Advanced Photon Source. GM/CA CAT has been funded in whole or in part with federal funds from the National Cancer Institute (Y1-CO-1020) and the National Institute of General Medical Sciences (Y1-GM-1104). Use of the Advanced Photon Source was supported by the U.S. Department of Energy, Basic Energy Sciences, Office of Science, under Contract DE-AC02-06CH1135. The isothermal titration calorimeter used in this work was supported by NSF Grant MRI 0723278.

REFERENCES

1. Ballou, D. P., Entsch, B., and Cole, L. J. (2005) Dynamics involved in catalysis by single-component and two-component flavin-dependent aromatic hydroxylases. *Biochem. Biophys. Res. Commun. 338*, 590–598.
2. van Berkel, W. J. H., Kamerbeek, N. M., and Fraaije, M. W. (2006) Flavoprotein monooxygenases, a diverse class of oxidative biocatalysts. *J. Biotechnol. 124*, 670–689.
3. Massey, V. (1994) Activation of molecular oxygen by flavins and flavoproteins. *J. Biol. Chem. 269*, 22459–22462.
4. Gatti, D. L., Palfey, B. A., Lah, M. S., Entsch, B., Massey, V., Ballou, D. P., and Ludwig, M. L. (1994) The mobile flavin of 4-OH benzoate hydroxylase. *Science 266*, 110–114.
5. Entsch, B., and Vanberkel, W. J. H. (1995) Flavoprotein structure and mechanism. 1. Structure and mechanism of para-hydroxybenzoate hydroxylase. *FASEB J. 9*, 476–483.
6. Enroth, C., Neujahr, H., Schneider, G., and Lindqvist, Y. (1998) The crystal structure of phenol hydroxylase in complex with FAD and phenol provides evidence for a concerted conformational change in the enzyme and its cofactor during catalysis. *Structure 6*, 605–617.
7. Xu, D., Ballou, D. P., and Massey, V. (2001) Studies of the mechanism of phenol hydroxylase: Mutants Tyr289Phe, Asp54Asn, and Arg281-Met. *Biochemistry 40*, 12369–12378.
8. Wang, J., Ortiz-Maldonado, M., Entsch, B., Massey, V., Ballou, D., and Gatti, D. L. (2002) Protein and ligand dynamics in 4-hydroxybenzoate hydroxylase. *Proc. Natl. Acad. Sci. U.S.A. 99*, 608–613.
9. Laden, B. P., Tang, Y., and Porter, T. D. (2000) Cloning, heterologous expression, and enzymological characterization of human squalene monooxygenase. *Arch. Biochem. Biophys. 374*, 381–388.
10. Buch, K., Stransky, H., and Hager, A. (1995) FAD is a further essential cofactor of the NAD(P)H and O_2-dependent zeaxanthin-epoxidase. *FEBS Lett. 376*, 45–48.
11. Hartmans, S., van der Werf, M. J., and de Bont, J. A. (1990) Bacterial degradation of styrene involving a novel flavin adenine dinucleotide-dependent styrene monooxygenase. *Appl. Environ. Microbiol. 56*, 1347–1351.
12. Panke, S., Witholt, B., Schmid, A., and Wubbolts, M. G. (1998) Towards a biocatalyst for (S)-styrene oxide production: Characterization of the styrene degradation pathway of *Pseudomonas sp*. strain VLB120. *Appl. Environ. Microbiol. 64*, 2032–2043.
13. Hollmann, F., Lin, P. C., Witholt, B., and Schmid, A. (2003) Stereospecific biocatalytic epoxidation: The first example of direct regeneration of a FAD-dependent monooxygenase for catalysis. *J. Am. Chem. Soc. 125*, 8209–8217.
14. Otto, K., Hofstetter, K., Rothlisberger, M., Witholt, B., and Schmid, A. (2004) Biochemical characterization of StyAB from *Pseudomonas sp*. strain VLB120 as a two-component flavin-diffusible monooxygenase. *J. Bacteriol. 186*, 5292–5302.
15. Kantz, A., Chin, F., Nallamothu, N., Nguyen, T., and Gassner, G. T. (2005) Mechanism of flavin transfer and oxygen activation by the two-component flavoenzyme styrene monooxygenase. *Arch. Biochem. Biophys. 442*, 102–116.
16. Panke, S., Wubbolts, M. G., Schmid, A., and Witholt, B. (2000) Production of enantiopure styrene oxide by recombinant *Escherichia coli* synthesizing a two-component styrene monooxygenase. *Biotechnol. Bioeng. 69*, 91–100.
17. Schmid, A., Hofstetter, K., Feiten, H. J., Hollmann, F., and Witholt, B. (2001) Integrated biocatalytic synthesis on gram scale: The highly enantio selective preparation of chiral oxiranes with styrene monooxygenase. *Adv. Synth. Catal. 343*, 732–737.
18. Jeffers, C. E., Nichols, J. C., and Tu, S. C. (2003) Complex formation between *Vibrio harveyi* luciferase and monomeric NADPH:FMN oxidoreductase. *Biochemistry 42*, 529–534.
19. Abdurachim, K., and Ellis, H. R. (2006) Detection of protein-protein interactions in the alkanesulfonate monooxygenase system from *Escherichia coli*. *J. Bacteriol. 188*, 8153–8159.
20. Campbell, Z. T., and Baldwin, T. O. (2009) Two lysine residues in the bacterial luciferase mobile loop stabilize reaction intermediates. *J. Biol. Chem. 284*, 32827–32834.
21. Sucharitakul, J., Phongsak, T., Entsch, B., Svasti, J., Chaiyen, P., and Ballou, D. P. (2007) Kinetics of a two-component p-hydroxyphenylacetate hydroxylase explain how reduced flavin is transferred from the reductase to the oxygenase. *Biochemistry 46*, 8611–8623.
22. Galan, B., Diaz, E., Prieto, M. A., and Garcia, J. L. (2000) Functional analysis of the small component of the 4-hydroxyphenylacetate 3-monooxygenase of *Escherichia coli* W: A prototype of a new Flavin:NAD(P)H reductase subfamily. *J. Bacteriol. 182*, 627–636.
23. Louie, T. M., Xie, X. S., and Xun, L. (2003) Coordinated production and utilization of $FADH_2$ by NAD(P)H-flavin oxidoreductase and 4-hydroxyphenylacetate 3-monooxygenase. *Biochemistry 42*, 7509–7517.
24. Otwinoski, Z., and Minor, W. (1997) Processing of X-ray diffraction data collected in oscillation mode. *Methods Enzymol. 276*, 307–326.
25. Vonrhein, C., Blanc, E., Roversi, P., and Bricogne, G. (2007) Automated structure solution with autoSHARP. *Methods Mol. Biol. 364*, 215–230.
26. de la Fortelle, E., and Bricogne, G. (1997) Maximum-likelihood heavy-atom parameter refinement for multiple isomorphous replacement and multiwavelength anomalous diffraction methods. *Methods Enzymol. 276*, 472–494.
27. Schneider, T. R., and Sheldrick, G. M. (2002) Substructure solution with SHELXD. *Acta Crystallogr. D58*, 1772–1779.
28. Abrahams, J. P., and Leslie, A. W. G. (1996) Methods used in the structure determination of bovine mitochondrial F1 ATPase. *Acta Crystallogr. D52*, 30–42.
29. Cowtan, K. (2006) The Buccaneer software for automated model building. 1. Tracing protein chains. *Acta Crystallogr. D62*, 1002–1011.
30. Emsley, P., and Cowtan, K. (2004) Coot: Model-building tools for molecular graphics. *Acta Crystallogr. D60*, 2126–2132.
31. Murshudov, G. N., Vagin, A. A., and Dodson, E. J. (1997) Refinement of macromolecular structures by the maximum-likelihood method. *Acta Crystallogr. D53*, 240–255.
32. McCoy, A. J., Grosse-Kunstleve, R. W., Adams, P. D., Winn, M. D., Storoni, L. C., and Read, R. J. (2007) Phaser crystallographic software. *J. Appl. Crystallogr. 40*, 658–674.
33. Laskowski, R. A. (1993) PROCHECK: A program to check the stereochemical quality of protein structures. *J. Appl. Crystallogr. 26*, 283–291.
34. Delano, W. L. (2002) The PyMOL molecular graphics system, DeLano Scientific, San Carlos, CA.
35. Collaborative Computational Project, Number 4 (1994) The CCP4 suite programs for protein crystallography. *Acta Crystallogr. D50*, 760–763.
36. Krissnel, E., and Henrick, K. (2004) Secondary-structure matching (SSM), a new tool for fast protein structure alignment in three dimensions. *Acta Crystallogr. D60*, 2256–2268.
37. Dundas, J., Ouyang, Z., Tseng, J., Binkowski, A., Turpaz, Y., and Liang, J. (2006) CASTp: Computed atlas of surface topograhy of proteins with structural and topographical mapping of functionally annotated residues. *Nucleic Acids Res. 34*, W116–W118.
38. Bond, C. S., and Schüttelkopf, W. (2009) ALINE: A WYSIWYG protein-sequence alignment editor for publication-quality alignments. *Acta Crystallogr. D65*, 510–512.
39. Holm, L., Kaariainen, S., Rosenstrom, P., and Schenkel, A. (2008) Searching protein structure databases with DaliLite v.3. *Bioinformatics 24*, 2780–2781.
40. Alfieri, A., Fersini, F., Ruangchan, N., Prongjit, M., Chaiyen, P., and Mattevi, A. (2007) Structure of the monooxygenase component of a two-component flavoprotein monooxygenase. *Proc. Natl. Acad. Sci. U.S.A. 104*, 1177–1182.
41. Kim, S. H., Hisano, T., Takeda, K., Iwasaki, W., Ebihara, A., and Miki, K. (2007) Crystal structure of the oxygenase component (HpaB) of the 4-hydroxyphenylacetate 3-monooxygenase from *Thermus thermophilus* HB8. *J. Biol. Chem. 282*, 33107–33117.
42. Eppink, M. H., Bunthol, C., Schreuder, H. A., and van Berkel, W. J. (1999) Phe161 and Arg166 variants of *p*-hydroxybenzoate hydroxylase. Implications for NADPH recognition and structural stability. *FEBS Lett. 443*, 251–255.

43. Ryan, K. S., Howard-Jones, A. R., Hamill, M. J., Elliott, S. J., Walsh, C. T., and Drennan, C. L. (2007) Crystallographic trapping in the rebeccamycin biosynthetic enzyme RebC. *Proc. Natl. Acad. Sci. U.S.A. 104*, 15311–15316.
44. Wierenga, R. K., De Jong, R. J., Kalk, K. H., Hol, W. G. J., and Drenth, J. (1979) Crystal structure of *p*-hydroxybenzoate hydroxylase. *J. Mol. Biol. 131*, 55–73.
45. Schreuder, H. A., Prick, P. A., Wierenga, R. K., Vriend, G., Wilson, K. S., Hol, W. G., and Drenth, J. (1989) Crystal structure of the *p*-hydroxybenzoate hydroxylase-substrate complex refined at 1.9 Å resolution. Analysis of the enzyme-substrate and enzyme-product complexes. *J. Mol. Biol. 208*, 679–696.
46. Hiromoto, T., Fujiwara, S., Hosokawa, K., and Yamaguchi, H. (2006) Crystal structure of 3-hydroxybenzoate hydroxylase from *Comamonas testosteroni* has a large tunnel for substrate and oxygen access to the active site. *J. Mol. Biol. 364*, 878–896.
47. Feenstra, K. A., Hofstetter, K., Bosch, R., Schmid, A., Commandeur, J. N., and Vermeulen, N. P. (2006) Enantioselective substrate binding in a monooxygenase protein model by molecular dynamics and docking. *Biophys. J. 91*, 3206–3216.
48. Entsch, B., Cole, L. J., and Ballou, D. P. (2005) Protein dynamics and electrostatics in the function of *p*-hydroxybenzoate hydroxylase. *Arch. Biochem. Biophys. 433*, 297–311.
49. Frederick, K. K., Ballou, D. P., and Palfey, B. A. (2001) Protein dynamics control proton transfers to the substrate on the His72Asn mutant of *p*-hydroxybenzoate hydroxylase. *Biochemistry 40*, 3891–3899.
50. Weber, F. J., Ooijkaas, L. P., Schemen, R. M., Hartmans, S., and de Bont, J. A. (1993) Adaptation of *Pseudomonas putida* S12 to high concentrations of styrene and other organic solvents. *Appl. Environ. Microbiol. 59*, 3502–3504.